FIMH 2021 Benchmark

January 28, 2021

Main additions/changes in version v1

1. Information on the computational phantom data has been updated, please see section 3.1 for detailed description of the computational phantom.

2. Computational phantom DICOM files have been uploaded to the GitHub repository BenchmarkData. Participants should analyze the DICOM images directly. Previous .mat and .dns files have been removed from the repository.

3. The output description has been updated.

4. Task for participants: please download the DICOM images for the computational phantom and import the images to your preferred analysis platform to ensure the DICOM images can be successfully loaded. If not, please notify the organizers: Vicky Wang (emailvywang66@stanford.edu) and Luigi Perotti (Luigi.Perotti@ucf.edu).

The goals of this benchmark are: 1) discussing the variability in calculation of cardiac kinematics (displacements and strains); 2) validating kinematics analysis tools using a computational phantom; 3) comparing strains and displacements computed from pre-clinical swine data across different analysis tools; and 4) improving our confidence in cardiac strain estimates as an imaging biomarker to distinguish between healthy and diseased hearts.

We want to emphasize that this benchmark is *not* meant as a challenge but simply as a platform for discussion and comparison to improve the calculation of cardiac motion and strains.

This working document is organized as follow:

1. Motivation

2. Method

3. Description of input data

1 Motivation

Cardiac strains have increasingly become a potential imaging biomarker to characterize cardiac function in health and disease. However, a large range of cardiac strains is reported in the literature, even for healthy volunteers. Several factors could contribute to this large spread, among which the processing methods adopted to compute cardiac strains from acquired displacements. As acquired displacement imaging data are inherently noisy, different processing methods may amplify or reduce the experimental error as well as introduce a bias in the computed strains.

In order to improve our confidence in using cardiac strains as biomarkers for cardiac function and dysfunction and compare strains reported in different studies, it is necessary to evaluate the variability introduced by different processing methods. To this end, the goal of this benchmark study is to characterize cardiac strains — particularly end systolic (ES) strains — variation due to different processing methods and pipelines.

2 Method

We propose to analyze three sets of cine DENSE (Displacement Encoding with Stimulated Echoes) data, from which cardiac strains are computed and compared across participants.

Each participant can use their preferred analysis tool to analyze the input data listed below. The open source cine DENSE post-processing toolbox found at cine DENSE analysis tool [1] can also be used as a starting point to analyze the input data.

Strain results will then be collected according to the guidelines provided in the "Description of selected output data for comparison" section listed below and summarized by the benchmark organizers.

3 Description of input data

Three sets of input data are provided: 1) synthetic cine DENSE data generated from a computational cylindrical phantom in which displacements are analytically defined such that exact analytical strains are also known; 2) mid-ventricular cine DENSE images for $N = 2$ healthy swine subjects ($Tr - 1242$ and $Tr - 1264$); and 3) mid-ventricular cine DENSE images for $N = 2$ swine subjects with an infarct ($Tr - 1434$ and $Tr - 1493$).

The data can be downloaded from: BenchmarkData

3.1 Computational phantom

Synthetic cine DENSE imaging data are generated from a computational cylindrical phantom whose deformation is analytically defined so that exact analytical displacements and strains can be computed

3.1.1 Computational phantom: Analytical motion

In this benchmark, we prescribed a deformation field in cylindrical coordinates of the form:

$$r(R, \Theta, Z) = a_1 + (1 + a_2)R + a_3 R^2 \; ; \tag{1a}$$

$$\theta(R, \Theta, Z) = \Theta + a_4 \frac{Z - Z_{\text{bot}}}{Z_{\text{top}} - Z_{\text{bot}}} \; ; \tag{1b}$$

$$z(R, \Theta, Z) = (1 + a_5)Z \; , \tag{1c}$$

where the values of the parameters a_1 to a_5 and the physical dimension of the phantom are reported in tables 1 and 2, respectively.

Table 1: Computational phantom deformation parameters.

a_1	a_2	a_3	a_4	a_5
-21.301899	0.875377	-0.009475	0.079924	-0.141489

Table 2: Computational phantom geometrical dimensions and synthetic myofiber preferential orientation at endo (inner), mid, and epi (outer) phantom surfaces

$R_{\text{endo}}[\text{mm}]$	$R_{\text{epi}}[\text{mm}]$	$Z_{\text{bot}}[\text{mm}]$	$Z_{\text{top}}[\text{mm}]$
25	35	0	28
$\theta_{\text{inner}}[\text{deg}]$	$\theta_{\text{mid}}[\text{deg}]$	$\theta_{\text{outer}}[\text{deg}]$	
70	-6	-42	

From eq. 1, the deformation gradient tensor $\mathbf{F}$ can be computed analytically, for example following the notes available here. Subsequently, the Green-Lagrange strain tensor can also be analytically computed from the deformation gradient tensor $\mathbf{F}$.

3.1.2 Computational phantom: synthetic cine DENSE DICOM images

The DICOM files corresponding to three short axis slices are provided. The bottom face of the phantom is fixed in Z ($Z_{\text{bot}} = 0\,\text{mm}$) and the short axis slices locations are $Z = 4\,\text{mm}$, $Z = 12\,\text{mm}$, and $Z = 20\,\text{mm}$. The following parameters are used to convert the phantom displacement field to three sets of phase images and magnitude images: $2.5 \times 2.5\,\text{mm}^2$ in plane resolution, $8\,\text{mm}$ slice thickness, $k_e = 0.08\,\text{cycles/mm}$ for all three phase encoding directions, the acquisition matrix size is 32×32.

Watermarks are added in the bottom right corner of the magnitude and phase images to ensure images are oriented correctly upon data loading. An increasing watermark length
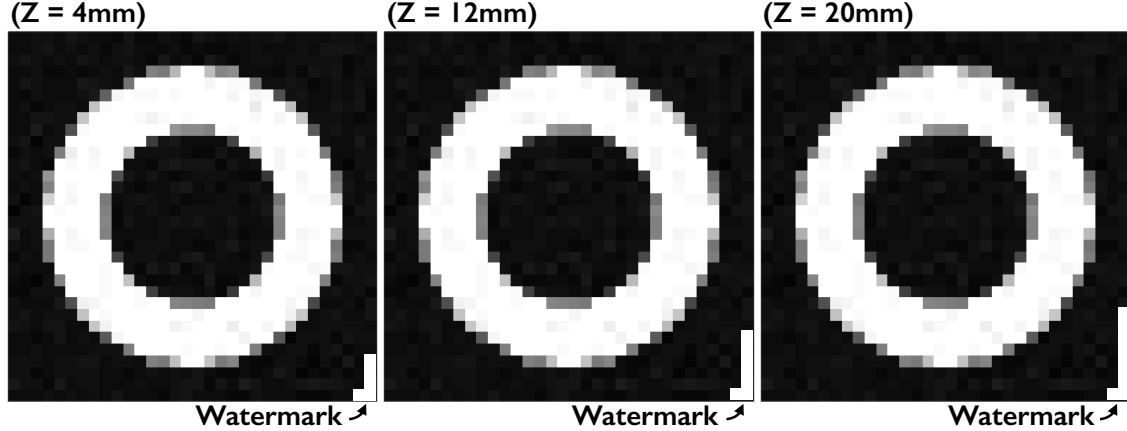
Figure 1: A watermark indicates the bottom right corner of the images. An increasing watermark length along the right vertical edge of the image corresponds to images at increasingly higher Z location, e.g., $Z = 4\,\text{mm}$, $Z = 12\,\text{mm}$, and $Z = 20\,\text{mm}$.

along the right vertical edge of the image corresponds to images at increasingly higher Z location (see Fig. 1).

Additional information about the computational phantom can be found in [2], although the parameters and the deformation equations reported here should be used as reference.
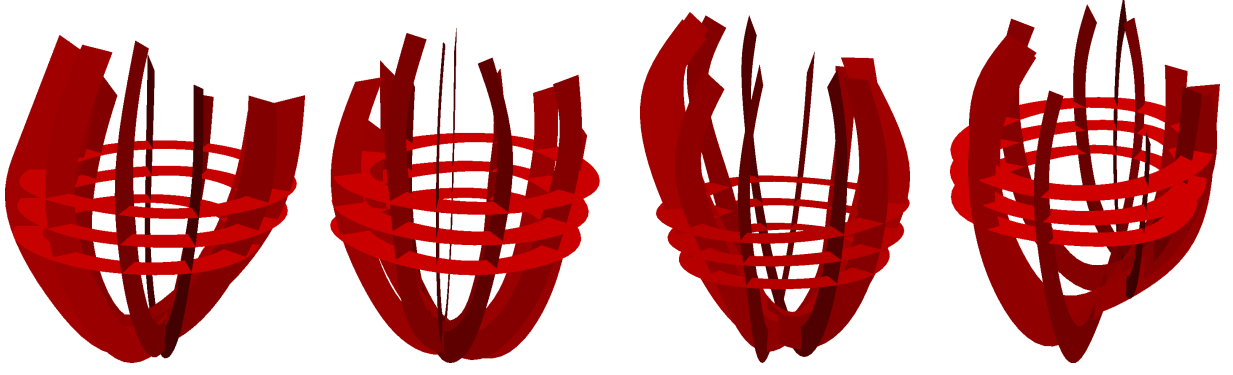
3.2 Healthy subjects

Cine DENSE data was acquired using a 3T (Prisma, Siemens) scanner following animal protocol #2015-124 as approved by the UCLA Chancellor's Animal Research Committee. Three mid-ventricular, 8 mm apart, cine DENSE short axis slices are provided per subject using the following sequence parameters: 15 ms view shared temporal resolution, $2.5 \times 2.5\,\text{mm}^2$ in plane resolution, balanced 4-point phase encoding in x, y, z, TE/TR $= 1.04/15$, $k_e = 0.08$ cycles/mm, $N_{\text{avg}} = 3$, spiral interleaves $= 10$.

An image of the location of the cine DENSE short axis slices for subjects $Tr - 1242$ and $Tr - 1264$ is reported in Fig. 2.

Conventional cine cardiac magnetic resonance (CMR) short axis images are also included for reference. The cine CMR images are acquired with a different temporal resolution, early on during the MR exams, and in some cases with a different trigger delay. Therefore there is no frame-to-frame correspondence between cine DENSE and cine CMR images. If segmentation is performed on the cine CMR images, care should be exerted in temporal alignment between cine DENSE and cine CMR images.

3.3 Subjects with myocardial infarct

Animal care and handling followed protocol #2015-124 as approved by the UCLA Chancellor's Animal Research Committee. In subject $Tr - 1434$, the infarct was due to a thrombus formed in the proximal left anterior descending (LAD) coronary artery. In subject $Tr - 1493$, an infarct was induced by injecting $2.5 - 3.0$ml of microspheres (Polybead, Polystyrene 90

(a) Subject $Tr-1242$.   (b) Subject $Tr-1264$.   (c) Subject $Tr-1434$.   (d) Subject $Tr-1493$.

Figure 2: Short axis slices location for healthy subjects $Tr-1242$ and $Tr-1264$, and for subjects $Tr-1434$ and $Tr-1493$ with myocardial infarction.

micron from Polysciences Inc) in a sub-branch of the left circumflex (LCx) coronary artery. The post-infarction MRI exam was performed eight weeks after infarct induction.

Cine DENSE short axis slices parameters are identical to the ones used in the MR exams of the healthy subjects. An image of the location of the DENSE MRI short axis data for subjects $Tr-1434$ and $Tr-1493$ with myocardial infarction is reported in Fig. 2.

Short axis cine images are also included for reference (Please see Healthy subjects description for more details.)

4   Description of selected output data for comparison

Once the participants have finished analyzing the cine DENSE images, strain and displacement estimates will be compared across different approaches. A pre-populated spreadsheet will be made available to the participants to collect and provide their results.

We will focus our comparison on: 1) the Lagrangian displacement of a set of 3D evenly spaced spatial points (0.5mm spacing in x, y, and z); and 2) average sector-based and transmural strains (E_{cc}, E_{ll}, and E_{rr}) for both computational phantom and pre-clinical swine data.

Table 3 contains a preliminary list of strain measures to be collected according to the guidelines below:

- Each entry should report median [$25^{th} - 75^{th}$ percentiles].

- The endocardial (endo), midwall (mid), and epicardial (epi) regions are defined by dividing the wall in 3 equal transmural segments.

- At every point X_q in a short axis slice, the radial direction is defined along the line joining X_q with the short axis slice barycenter (see Fig. 3A).

- At every point X_q in a short axis slice, the circumferential direction is defined along the line perpendicular to the radial direction (see Fig. 3A).

	Endo	Mid	Epi	R1	R2	R3	R4	R5	R6	Total
E_{cc}										
E_{ll}										
E_{rr}										
E_{ff}										

Table 3: Strain output measures

- The longitudinal direction is identified as perpendicular to the short axis slice plane (see Fig. 3A).

- Regional strains should also be collected across slices. Six regions are defined as follow, recalling the six mid-ventricular AHA regions. On each slice, the right-ventricle (RV) insertion points P1 and P2 are identified together with the barycenter of the left ventricle. The septal region contained between points P1 and P2 is subdivided into two equal regions (R1 and R2) spanning the same angle with respect to the LV barycenter. The remaining of the myocardial wall is subdivided into four equal regions (R3 to R6) spanning the same angle with respect to the LV barycenter (See Fig 3C).

- E_{vv} represent the strain computed by projecting the Green-Lagrange strain tensor $\mathbf{E}$ along the direction $\mathbf{v}$, where $\mathbf{v}$ can represent the circumferential direction $\mathbf{c}$, radial direction $\mathbf{r}$, and longitudinal direction $\boldsymbol{\ell}$ along the $\mathbf{z}$ axis in the reference configuration.

- The calculation of myofiber strains is optional. If participants decide to compute myofiber strains, at each location the "myofiber" direction is defined in the plane identified by the circumferential and longitudinal directions and forming an helix angle α with the short axis plane. The helix angle α is rule based and varying quadratically from 70° at endocardium, to 0° at midwall, and −50° at epicardium.

- All strains and displacement measures are sampled at the centers of the voxels defined by a grid with in plane resolution equal to 0.5 mm. The grid covers the entire image short axis plane and only voxels in the myocardium at the reference configuration will be considered (see Fig. 3B).

In addition to Table 3, the following output measures should be reported:

1. For the computational phantom only, the norm of the difference between analytical and computed displacements per each short axis slice;

2. E_{cc}, E_{ll}, and E_{rr} strain maps for the mid short axis slices for each analyzed subject.

The first phase recorded in the DENSE data will be used as reference configuration.

Peak systole is identified as the cardiac phase where E_{cc} is maximum. Although peak systole may be identified in several different ways, this criterion is chosen to have a common standard to report the data for comparison across different participants.
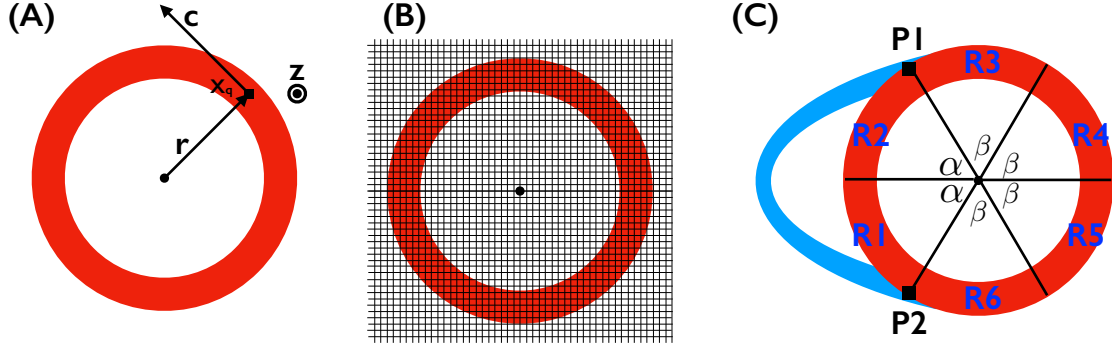
Figure 3: (A) Cylindrical coordinates system used to project the strain tensor **E** along the radial, circumferential, and longitudinal directions. (B) Schematic of sample grid overlaid to short axis slice. (C) Regional subdivision per slice.

5 Dissemination of the cardiac kinematics benchmark study

We are actively working with *Philosophical Transactions A* to host a special issue on this benchmark study. More details will be available soon.

References

[1] Bruce S Spottiswoode, Xiaodong Zhong, Aaron T Hess, CM Kramer, Ernesta M Meintjes, Bongani M Mayosi, and Frederick H Epstein. Tracking myocardial motion from cine DENSE images using spatiotemporal phase unwrapping and temporal fitting. *IEEE transactions on medical imaging*, 26(1):15–30, 2007.

[2] Ilya A Verzhbinsky, Luigi E Perotti, Kévin Moulin, Tyler E Cork, Michael Loecher, and Daniel B Ennis. Estimating aggregate cardiomyocyte strain using in vivo diffusion and displacement encoded MRI. *IEEE Transactions on Medical Imaging*, 39(3):656–667, 2019.